Lattice-Boltzmann simulation of solvent diffusion into oil-saturated porous media

Can Ulas Hatiboglu and Tayfun Babadagli*

Department of Civil and Environmental Engineering, School of Mining and Petroleum, University of Alberta, 3-112 Markin CNRL-NREF, Edmonton, AB, Canada T6G 2W2

(Received 1 March 2007; revised manuscript received 20 October 2007; published 13 December 2007)

We simulated the diffusion process into oil-saturated porous media using the modified diffusion-limited aggregation and the lattice Boltzmann method algorithms. The results were matched to visual experiments for cocurrent (two sides of the model open to flow) and countercurrent (only one side of the model open to flow) diffusion for horizontally and vertically positioned samples. The model saturated with oil was exposed to pentane in order for a miscible interaction to take place. These experiments mimic the transfer between the rock matrix and fracture during gas or liquid solvent injection for enhanced oil recovery, underground waste disposal, groundwater contamination, and CO_2 sequestration in naturally fractured reservoirs. Finger development at the early stages of the process was controlled by oil viscosity and the interaction type dictated by the boundary conditions. The convective transport driven by the buoyancy that was experimentally observed on vertically oriented samples and transfer driven by diffusion on the horizontal ones were captured in the LBM simulation of the process.

DOI: 10.1103/PhysRevE.76.066309 PACS number(s): 47.55.P−, 66.30.−h, 47.56.+r

I. INTRODUCTION

Investigations on the physics of the mass transfer between the rock matrix and fracture are important in different engineering practices such as exploitation of oil and gas, CO_2 sequestration, and groundwater contamination in naturally fractured reservoirs. Stochastic models have been commonly applied recently to simulate different types of displacement processes in porous media. Studies in this area resulted in different displacement patterns varying from pistonlike to fingering [1]. Quasistatic displacement dominated by the capillary forces yields a process called invasion percolation (IP) [2,3]. Diffusion-limited aggregation (DLA) patterns were obtained during diffusion- and viscous-force-dominated processes [4]. In contrast to stochastic models, the lattice Boltzmann method (LBM) is relatively new and promising [5–9]. The underlying idea of the LBM is to construct simplified kinetic models that incorporate the important physics of microscopic processes so that averaged properties obey the desired macroscopic equations.

Modifications to IP and DLA algorithms were developed to better simulate the flow in pore level. Biroljev *et al.* [10] took the gravity effect into account, developed a computer model, and tested the model experimentally. They concluded that the front between the fluids was found to scale with the dimensionless Bond number (ratio between gravitational and capillary forces), and the fractal dimension of the profile was found to be $D_e \approx 1.34$.

In a recent study, Ferer *et al.* [11] showed that the IP models are applicable to the systems in the limit of zero capillary number whereas the DLA models the flow in the limit of zero-viscosity ratio. Fernandez *et al.* [12] defined the crossover length from invasion percolation to diffusion-limited aggregation in porous media. Interpore surface tension was neglected in their study and the invading fluid was assumed to be nonviscous.

Evolution of the LBM was observed as well over the last decade. Research was focused on improving the algorithm to simulate fluids both miscible and immiscible, as well as more efficient algorithms to lighten the heavy computing requirements. Bouzidi *et al.* [13] studied the velocity boundary condition for curved boundaries in an effort to improve the simple bounce-back boundary condition. They worked on LBM boundary conditions for moving boundaries by combination of the "bounce-back" scheme and spatial interpolations of first and second order. Flekkoy [14] was the first to use the Bhatnagar-Gross-Krook model for miscible fluids. He derived the convection-diffusion equation and the Navier-Stokes equation describing the macroscopic behavior using the Chapman-Enskog expansion. Stockman *et al.* [15] focused on enhancing the algorithm and making it more efficient for practical use and used the code to model dispersion in rough fractures and double-diffusive fingering. The LBM is also useful to model immiscible fluid flow [12]. Introducing interfacial tension phenomena and the interface between the fluids, one can model phase-separating fluids. An important topic in multiphase flow, bubble motion under gravity, was modeled by Takada *et al.* [16]. They were able to obtain realistic results that can simulate bubble coalescence and bubble motion with surface tension values that can satisfy the Laplace's law.

Experimental studies on the miscible displacement processes are limited especially from the visualization point of view. Recently, Hatiboglu and Babadagli presented observations on two-dimensional (2D) visualization models for cocurrent and countercurrent diffusion [17] also comparing with the core experiments [18]. They showed the importance of interaction type, viscosity of the displaced fluid, matrix boundary conditions, and displacement direction on the displacement process. They also observed that the continuum models fail to capture the physics controlling the process and stochastic models could be an alternative. The IP approach was useful in modeling the process if there was no gravity effect (horizontally positioned cases) [19].

*Corresponding author; tayfun@ualberta.ca

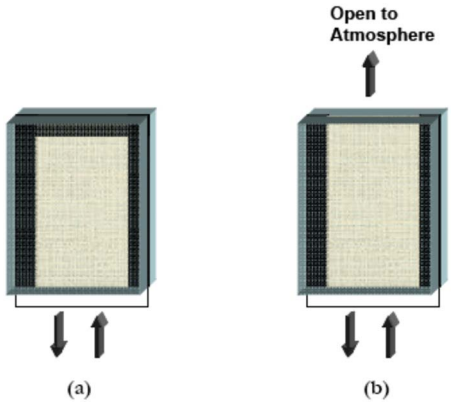

FIG. 1. (Color online) Schematic representation of the experimental model with different boundary conditions: (a) countercurrent and (b) cocurrent interactions.

In this study, both cocurrent and countercurrent diffusion into porous medium were studied visually under fully static conditions for different size models and fluid properties. Two-dimensional visual models were constructed of glass beads sandwiched between two acrylic sheets saturated with oil and placed into a tank filled with the displacing (diffusing) phase either vertically or horizontally. The process was modeled using first the DLA and then LBM methods. Both models take gravity and boundary conditions into account.

II. EXPERIMENTAL STUDY

For the visualization study, glass-bead-packed models were used. Transparent acrylic was chosen as enclosure material. The model is in a square shape with dimensions of 5 $\times 5$ cm^2. For one case, the 6×3 cm^2 model was used. To represent the porous media, glass beads with 0.1 mm diameter were chosen. The gap between the two layers of acrylic was measured to be 0.3 mm. The glass beads were packed densely and homogeneously. Filter paper on one end of the model was used for mechanically stabilizing the glass beads as well as ensuring a smooth edge for the diffusing phase to enter. The thickness of the model was kept minimal to ensure 2D behavior.

TABLE I. Fluid pairs used in experiments.

	Pentane	Kerosene	Mineral oil
Density (g/cc)	0.63	0.79	0.83
Viscosity (cp)	0.38	2.9	36.32
Diffusion coefficient (m^2/s)	0.084		

To be able to create boundary conditions, epoxy was decided to be the most appropriate material because of its inert behavior to solvent reactions. Three edges of the models were sealed with epoxy to ensure the fluid interaction occurs through only one side creating a countercurrent-type transfer [Fig. 1(a)]. Similarly, cocurrent models were obtained sealing only the two opposing sides [Fig. 1(b)]. The properties of the fluids used in the experiments are tabulated in Table I. The solvent phase (pentane) was dyed with red color to distinguish the difference. The oil samples were kept at its original color (yellowish white).

III. PROCEDURE

After constructing the glass bead models, they were saturated with oleic phase—namely, kerosene or mineral oil—under vacuum. Two slightly different setups were used for vertical and horizontally oriented experiments (Fig. 2). In both experimental cases, a continuous supply of solvent (pentane) was achieved using a micropump to feed the pentane container.

The light source is critical in obtaining good quality images. A high-intensity halogen lamp was chosen to be appropriate. But this had to be cooled off properly not to affect the experimental results. To assure this, a fan-cooled, computer-controlled illumination system was constructed. The system made it possible to turn the light off, while not capturing the image, to prevent the excess heat generation.

The cocurrent models (two sides sealed) for the horizontal orientation was difficult to perform since the edge open to atmosphere caused mechanical instability. To prevent this, the model was slightly tilted upwards so as to not to have any pentane contact with the upper portion of the model.

The visualization equipment consists of a 6.3MP DSLR

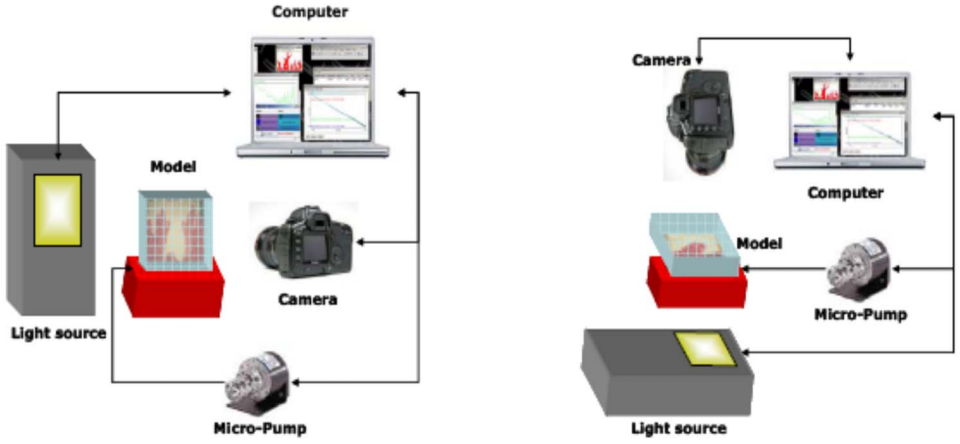

FIG. 2. (Color online) Experimental setup for (a) vertical and (b) horizontal orientations.

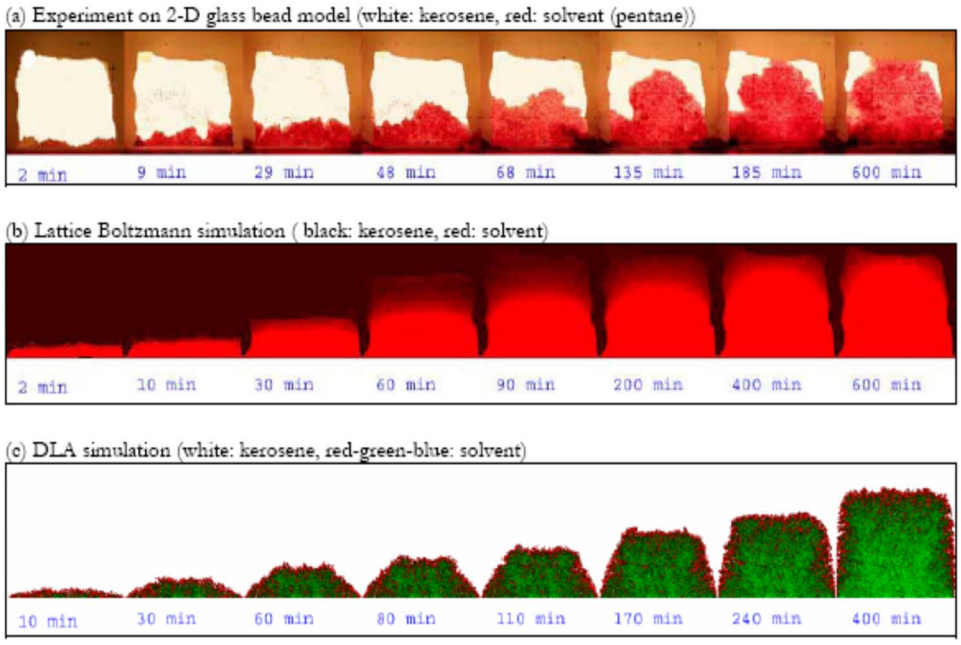

FIG. 3. (Color online) Kerosene-pentane diffusion for the countercurrent, horizontal case: (a) experimental observations, (b) LBM simulation, and (c) DLA simulation of the process. Model scale: 5×5 (cm^2).

camera, which was configured to do time-lapse photography. A small piece of code was written to synchronize the light source and the camera.

An open-source image-processing software (ImageJ) was used for capturing and processing of the images because of its multiimage tiff file-handling capability and ability to incorporate user-written codes through plug-ins.

IV. RESULTS

A. Horizontal experiments: Countercurrent interaction

For the countercurrent models, horizontal orientation showed a steady and frontal displacement in all cases [Figs. 3(a) and 4(a)]. Kerosene and mineral oil behavior was very similar, and the small fingers observed in the early stages of

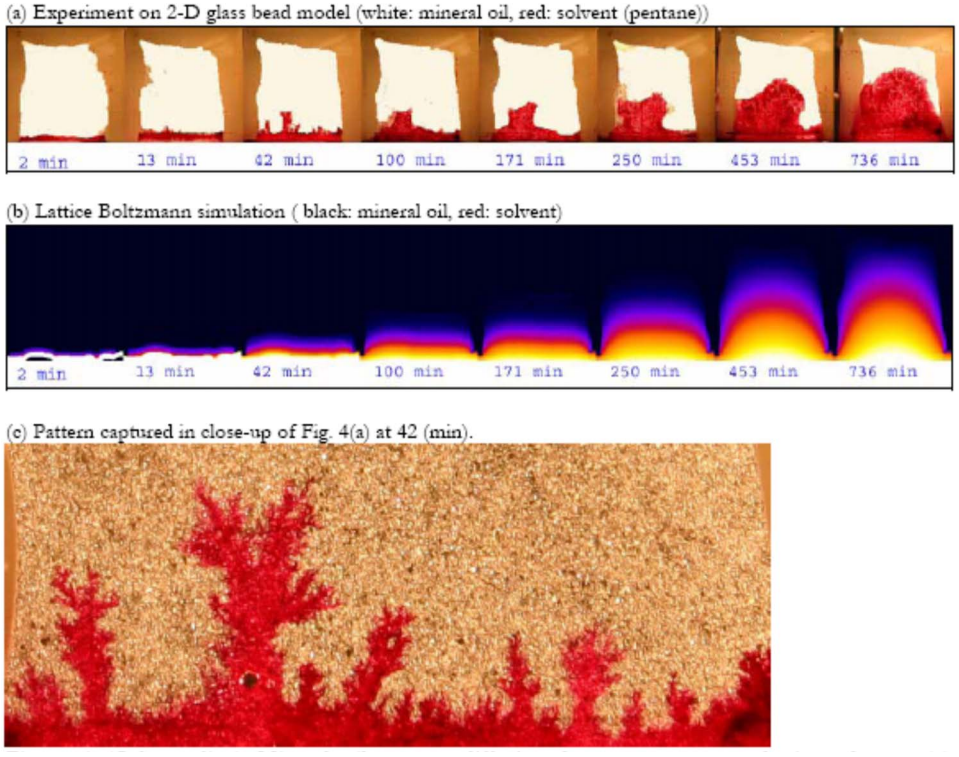

FIG. 4. (Color online) Mineral oil-pentane diffusion for the countercurrent, horizontal case: (a) experimental observations and (b) LBM simulation of the process. Model scale: 5×5 (cm^2).

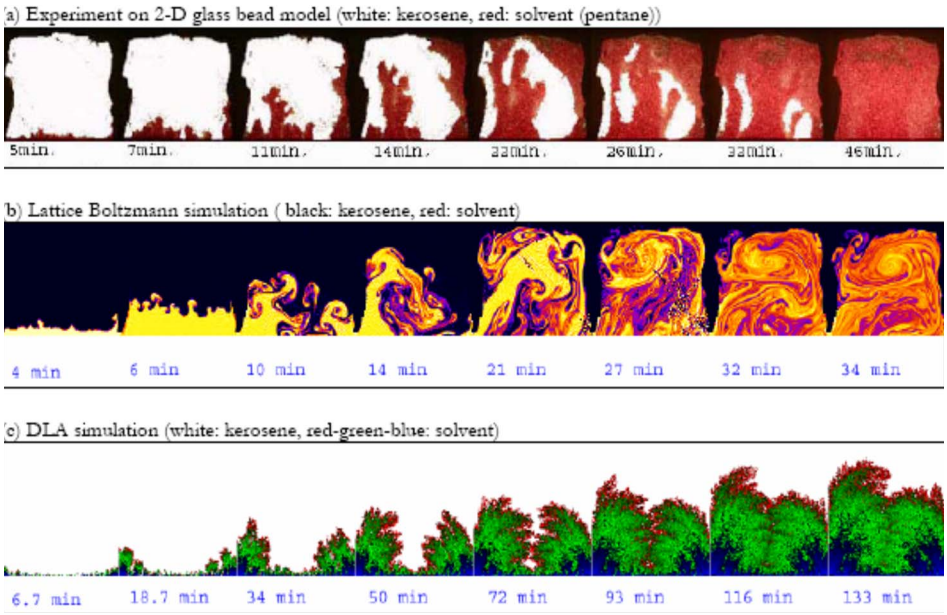

FIG. 5. (Color online) Kerosene-pentane diffusion for the countercurrent, vertical case: (a) experimental observations, (b) LBM simulation, and (c) DLA simulation of the process. Model scale: 5×5 (cm^2).

the process disappeared at the later stages. The viscosity difference translated into experiments as a time difference, less viscous kerosene having a faster process. The front progressed in the middle of the model was faster compared to the edges, creating a "bullet"-shaped profile.

When we zoom into the front of a pattern, we see DLA-type fingers more clearly at smaller (micro) scale. A close-up for the case in 42 min is given in Fig. 4(c). This was the motivation for using DLA modeling of the experiments as will be discussed in the next section.

B. Vertical experiments: Countercurrent interaction

When the gravity becomes effective, more complex patterns were observed. Buoyancy drive causes a convection dominated miscible displacement process. The kerosene case displayed a faster process than the mineral oil case caused by low resistance to flow due to low viscosity. Thinner fingers were observed in the kerosene experiments, causing an earlier arrival of the front at the top boundary [Fig. 5(a)]. The difference in viscosity is reflected as longer process times for the mineral oil case [Fig. 6(a)]. Fingers were developed through the sides of the models due to less resistance to flow caused by the inner pressure distribution. After the arrival of the front at the top boundary, a "convective" displacement due to the density difference between the distinguishable "phases" (original oil and oil mixed with pentane) began to dominate. The buoyant convection followed a path depicted in Fig. 7. The fluid fronts tend to progress close to the boundaries where less resistance exists compared to the center (in 90 min). Once the front reached the top of the model (in 200 min), the unswept oil in the middle portion was displaced predominantly by the "buoyant convection" where displacement develops through the sides of the sample and goes downward from the inner part as indicated by arrows. In other words, the convection took place from the outer sides of the model, and as the lighter phase accumulates on top of the model it displaces the unmixed—heavier—original oil down by a circular motion. That is an interesting characteristic of the diffusion phenomenon, and it was more prominent for the lighter oil case (kerosene).

C. Vertical experiments: Cocurrent

The cocurrent models have one edge open to atmosphere which alters the pressure distribution in the model. This

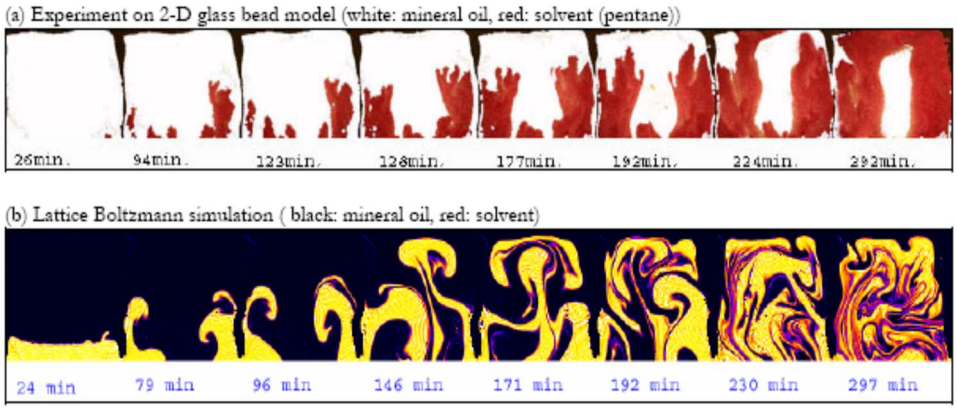

FIG. 6. (Color online) Mineral oil-pentane diffusion for the countercurrent, vertical case: (a) experimental observations and (b) LBM simulation of the process. Model scale: 5×5 (cm^2).

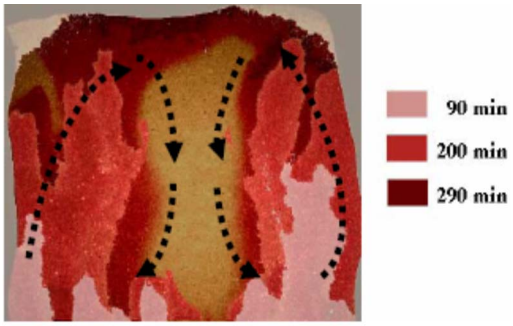

FIG. 7. (Color online) Convective behavior observed in vertical-oriented experiments.

change in the boundaries and, thereby the inner pressure distribution, caused radical differences on the displacement patterns compared to the countercurrent model.

The kerosene-pentane case showed a similar convection-type displacement to the equivalent case for the countercurrent interaction but with more distinctive fingered patterns [Fig. 8(a)]. An open top edge causes a more tolerant behavior in terms of oil downflow. This translates as a higher intrusion rate for the pentane phase and thus faster oil recovery. This yielded a faster convective displacement compared to the countercurrent equivalent of the case.

The experiments done with the mineral oil showed a bullet-shaped fluid front progressing centered along the model [Fig. 9(a)] without any significant fingering. Once the displacement front (mixture with lower density than original oil) reached the top of the model, accumulation on the top was observed as in the countercurrent cases and convective displacement due to buoyancy process started.

In all cases above where a square-shape model was used, the sealed edges of the model strongly dominated the displacement process and finger development. To minimize this effect the shape and the dimensions of the model was altered slightly. Figure 10(a) shows the countercurrent diffusion process on a rectangular-shape model for mineral oil. In the first 68 min, fingers developed similar to the square equivalent of this case [Fig. 6(a)]. Finger development through the sides was less compared to the square-shape model, but at later stages, convective transport was also observed.

V. EXPERIMENTAL LIMITATIONS

Hele-Shaw-type cells or parallel plates are widely used to observe different flow phenomena ranging from viscous fingering to double-diffusive convection for 2D analysis. Transparent plates provide an unobstructed view of the fluid front behavior, where in real porous media this would be hard to observe. Pringle *et al.* [20] used Hele-Shaw experiments to capture the structural patterns of double-diffusive convection. They have justified that parallel plates would also serve as an analog for flow through porous media provided that the assumptions by Wooding [21] are satisfied:

$$\frac{\langle b\rangle}{\delta} \ll 1, \quad \frac{V_c\langle b\rangle^2}{\delta v} \ll 1, \quad \frac{V_c\langle b\rangle^2}{\delta D} \ll 1,$$

where δ is the smallest length scale of motion (taken to be the horizontal length scale) and D the diffusivity. This criterion translates as the smallest length scale of motion to be much larger than the mean aperture. This criterion was satisfied within a small amount of time. The second criterion constraints the inertial effects to be negligible relative to viscous effects, and this criterion was satisfied in all experiments as they were conducted under fully static conditions. The third criterion limits momentum transfer to be negligible relative to diffusive transfer, which is the case in our experiments as there was no injection in the system and the process was totally controlled by diffusive and dispersive transport.

Although these constraints are satisfied, there are still other factors that make Hele-Shaw cells differentiate from real porous media, such as heterogeneity, presence of dead pores, etc. In an effort to incorporate porous medium characteristics, uniform-size glass beads are used as pore grains within the acrylic parallel plates.

It is confirmed that lattice Boltzmann simulations in three dimensions are more stable and also more accurate in modeling. In their simulations, Stockman *et al.* [15] observed that the three-dimensional (3D) nature of the field has been shown to influence fluid front evolution. On the downside, a 3D simulation would require more computational source and 3D experimental analysis for verification is considerably difficult.

Considering the size of the grains and pore sizes in our case, with the addition of the tortousity factor the flow would

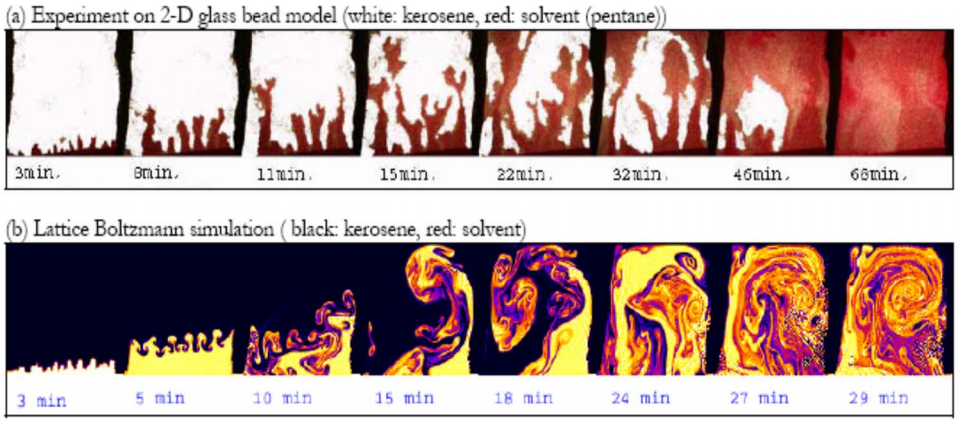

FIG. 8. (Color online) Kerosene-pentane diffusion for the cocurrent, vertical case: (a) experimental observations and (b) LBM simulation of the process. Model scale: 5×5 (cm^2).

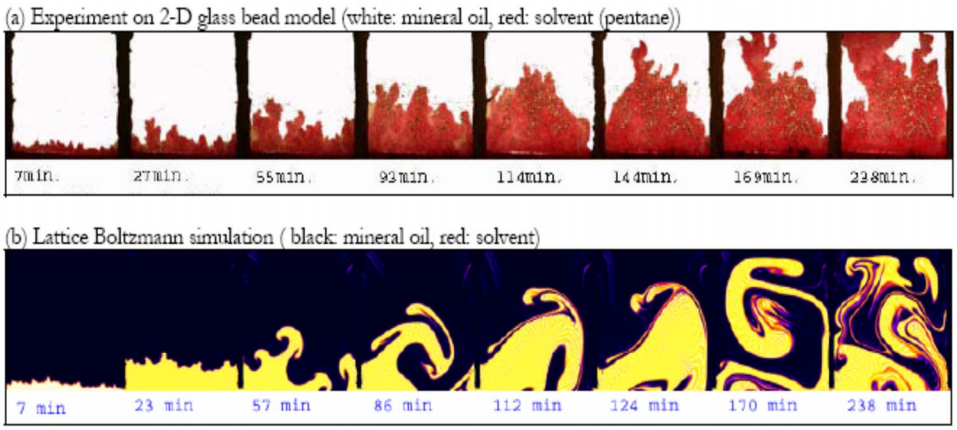

FIG. 9. (Color online) Mineral oil-pentane diffusion for the cocurrent, vertical case: (a) experimental observations and (b) LBM simulation of the process. Model scale: 5×5 (cm^2).

be similar to what it would be in a Hele-Shaw cell. In order to prevent further introduction of heterogeneity and complexity by including porous media in simulations, we decided to use the simplest porous medium structure.

Since the experiments conducted in this study are under static conditions and there is no injection of fluid involved, the overall momentum would be conserved. This study is aimed to show the abilities of LBM and our efforts in the area of scaling the simulations to real-life situations. For more realistic modeling, 3D cases with pore-medium representations could be chosen, but this would require considerably large matrix sizes and vast computational resources.

VI. MODELING

A. Lattice Boltzmann method

The LBM is simply composed of a set of nonlinear partial differential equations (the Navier-Stokes equations) which are ultimately a statement of mass and momentum conservation. The abilities of the method attracted attention not only because it can simulate fluid flow through complex boundaries and interfacial dynamics, but also it can easily be programmed for the parallel computers. A pioneering work by Kadanoff [5] justified the use of simplified kinetic-type methods for macroscopic fluid flows. It was shown that the macroscopic dynamics of a fluid is the result of the collective behavior of many microscopic particles in the system and that the macroscopic dynamics of a fluid is the result of the collective behavior of many microscopic particles in the system and that the macroscopic dynamics is not sensitive to the underlying details in microscopic physics.

Several review papers described the basics and evolution of the method over time [5–7,9]. Some researches focused on phase separation fluids [7,22,23]; others dealt with miscible processes [8,14,15,24–26].

Since the LBM is composed of distribution functions, physical interactions of the fluid particles (either one-phase or multiphase) can be conveniently incorporated. In the case of complex fluid flows with interfaces between multiple phases and phase transitions, the complex macroscopic behavior is the result of the interaction of the fluid particles in a microscopic level. Rothman and Keller [23] were the first to develop a lattice gas model for two immiscible fluids. The

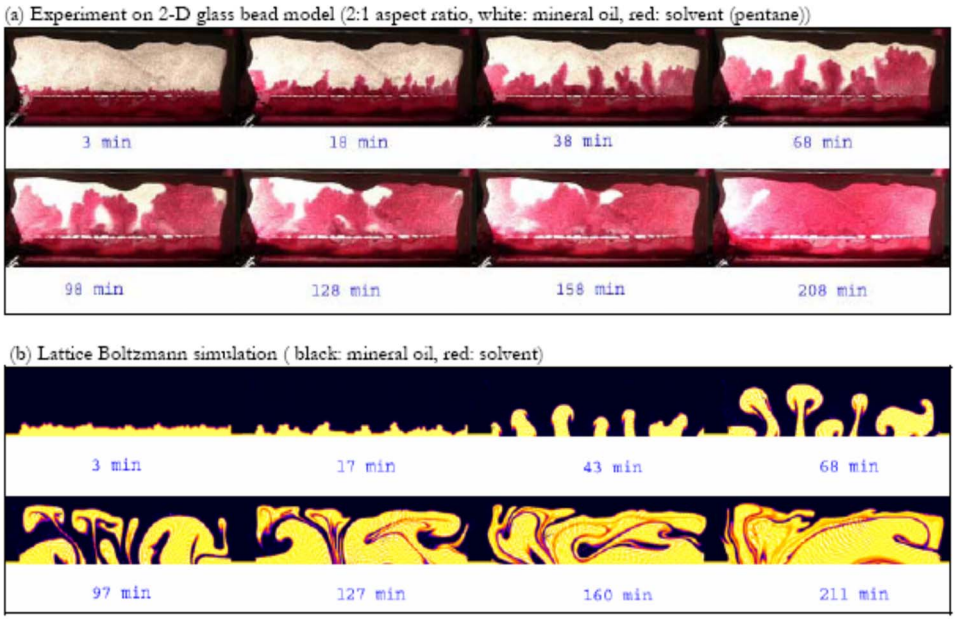

FIG. 10. (Color online) Mineral oil-pentane diffusion for the countercurrent, vertical case with 2:1 aspect ratio: (a) experimental observations and (b) LBM simulation of the process. Model scale: 6×3 (cm^2).

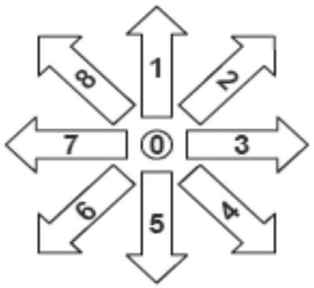

FIG. 11. Speed vectors used in the LBM simulations.

Boltzmann approach was later applied by Gunstensen *et al.* [22]. This approach used a rearranging of the particle distributions of the two species in the interfacial region depending on concentrations. The miscible fluid model was first proposed by Flekkoy [14] and Flekkoy *et al.* [27] in which the sum of the distribution functions of the two components and the difference between them are made to relax at difference rates. The relaxation rate is dependent on the kinematic viscosity for one of the distribution functions and diffusion coefficient for the other. Since different rates are used for relaxation, the diffusivity is independent of the viscosity of the fluid mixture.

The LBM proposed in this study uses a nine-speed structure in a square lattice which is widely expressed as D2Q9 (two dimensions, nine velocities). The fluids are distinguished using Flekkoy proposed method [14] as either "red" or "blue." The basic variables of the models are the distribution functions, where R_i is red (solvent) and B_i is blue (oil) fluid densities:

$$N_i = \mathrm{R}_i + B_i, \tag{1}$$

$$\Delta_i = \mathrm{R}_i - B_i, \tag{2}$$

where R_i (B_i) is the mean occupation number for red (blue) fluid particles in direction i at a given node. By choosing the variables in this manner, it is possible to decouple the information of flow (N_i) from the information of amount of solvent (Δ_i). The particles on each node have nine velocities (Fig. 11).

According to the kinetic equation of lattice-gas automata (LGA), particles in one node with a velocity e_i after a time step Δt would be conserved unless some collision occurs, which is depicted with the Ω function. Ω is called the collision operator. As a derivative method of the LGA, the LBM incorporates the same equation which is

$$N_i(x + c_i, t + 1) = N_i(x,t) + \lambda_r N_i^{neq}(x,t), \tag{3}$$

$$\Delta_i(x + c_i, t + 1) = \Delta_i(x,t) + \lambda_D \Delta_i^{neq}(x,t), \tag{4}$$

where this represents that the particles at node(x,t) move with unit speed c_i. Here λ_v and λ_D are the relaxation parameters which determine the kinematic viscosity v and the diffusion coefficient D, respectively. The relationship between those parameters is given as

$$v = \tfrac{1}{3}\left(\lambda_v - \tfrac{1}{2}\right), \tag{5}$$

$$D = \tfrac{1}{3}\left(\lambda_D - \tfrac{1}{2}\right). \tag{6}$$

The nonequilibrium distributions are given as

$$N_i^{neq} = N_i - N_i^{eq}, \tag{7}$$

$$\Delta_i^{neq} = \Delta_i - \Delta_i^{eq}, \tag{8}$$

where (for nine-speed architecture)

$$N_i^{neq} = wi\varrho(1 + 3c_i \cdot u + 9/2(c_i \cdot u)^2 - 3/2(u \cdot u)), \tag{9}$$

$$\Delta_i^{neq} = wi\varrho(1 + 3c_i \cdot u). \tag{10}$$

The mass density per site is defined as follows:

$$\rho = \sum_i N_i. \tag{11}$$

Then, the momentum density can be written as

$$\rho u = \sum_i c_i N_i. \tag{12}$$

The density difference ($\Delta\varrho = \varrho_r - \varrho_b - \varrho_r$ and ϱ_b are the site densities) of red (blue) particles is defined as

$$\Delta\rho = \sum_i \Delta_i. \tag{13}$$

The vectors c_i are velocity vectors on the lattice connecting neighboring nodes. On the square lattice one of these c_i's has zero length, four of them have unit length (vertical and horizontal vectors), and the remaining four have $\sqrt{2}$ length (diagonals) as depicted in Fig. 11. The weight factors (w_i) are chosen to obtain isotropy of velocity moments and depend only on the lengths of the c_i's:

$$w_i = \begin{cases} \frac{4}{9} \text{ for } i=0, \\ \frac{1}{9} \text{ for } i = (1,3,5,7), \\ \frac{1}{36} \text{ for } i = (2,4,6,8). \end{cases} \tag{14}$$

From Eq. (12), the flow is defined as

$$u = \frac{1}{\rho}\sum_i N_i c_i. \tag{15}$$

Until now the basic equations of the LBM are given. These equations are not designed to handle external body forces such as gravity. The gravity term has long been a subject of discussion in this field. Some researchers modified the velocity vector [25,28]; others have incorporated it as an additional term to the Boltzmann equation (into the collision function to be more specific [29,30]). Composite-hybrid models have also been proposed [31].

This study uses the method proposed by van der Sman [32] where the moments of the equilibrium distributions equal those of the Maxwell-Boltzmann distribution.

The Boussinesq approximation is used to model the natural convection caused by the density differences. An additional term F is added to the velocity vector as

$$u = \frac{1}{\rho}\sum_i N_i c_i + F, \tag{15a}$$

$$F = \rho_f g\left(1 - C_j \frac{\partial \rho_f}{\partial C_j}\right), \tag{16}$$

where ρ_f denotes the occupation number for the carrier fluid (oil), g is gravity, and C_j is the solvent concentration. The collision step [Eqs. (3) and (4)] is also changed to conform the Maxwell-Boltzmann constants:

$$N_i(x + c_i, t + 1) = N_i(x,t) + \lambda_v N_i^{neq}(x,t) + J, \tag{17}$$

$$J = -\rho_f g w_i \frac{c_i}{c_s^2} \Delta t, \tag{18}$$

where c_s is the speed of sound and c_i/c_s^2 equals 3 for D2Q9 geometry.

Because of the numerical constraints of the LBM, it is not possible to directly input the variables and, therefore, scaling has to be applied. It is known that the Rayleigh and Schmidt numbers (the Prandtl number for heat convection) are the controlling parameters for natural convection. The variables are scaled to match Rayleigh and Schmidt numbers for real-life values.

The Rayleigh number for this study is defined as

$$\mathrm{Ra} = \left[\left(\frac{\partial \rho_f}{\partial C_j}\right) C_j g \sin\theta \left(\frac{h^2}{12}\right) L\right] \Big/ Dv, \tag{19}$$

and the Schmidt number is

$$\mathrm{Sc} = \frac{v}{D}. \tag{20}$$

Since we are modeling a 3D phenomenon on a 2D model, we accepted h as 1 for the LBM; this parameter translates as the model thickness. L is the length term.

The real values of the oil viscosity, diffusion coefficient for solvent and oil, and gravity term were used to calculate the Ra and Sc numbers. Experimental values of the Rayleigh and Schmidt numbers were calculated to be 224.67 and 28.6, respectively. After entering the constraints in Solver option in MS Excell, scaled values of those three parameters were computed and used in the simulation.

Time values are obtained from number of iterations since each iteration step reflects an incremental time increase. To obtain the time values, for a healthy comparison, it has to be scaled back using the equation previously proposed by Stockman *et al.* [15] and van der Sman [32]:

$$(\mathrm{time}) = 12Lv/(h^2 g). \tag{21}$$

Following the initialization step, particles are streamed for the next step. Completion of streaming requires the calculation of new density, flow speed, and particle distribution values. Density and flow values are used to get the distribution in equilibrium.

The last step of the loop is the collision step, where particles collide depending on their relaxation parameter. The relaxation parameter for each phase is different, and they are obtained from viscosity and diffusion coefficient values. Instead of using simple bounce-back, the scheme that is proposed by Bouzidi *et al.* [13] is utilized for this study. This scheme is more appropriate for curved boundaries since it uses linear or quadratic interpolation formulas involving values at two or three nodes (Fig. 12).

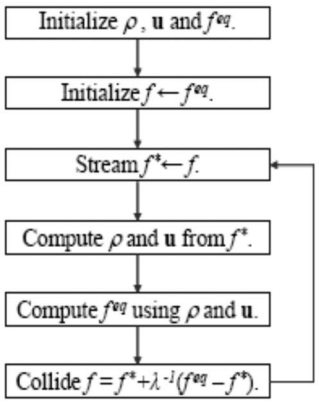

FIG. 12. Algorithm of the loop section.

To model the continuous solvent feed of the experimental model, the solvent feed is incorporated as a static reservoir at the bottom of the model. A small amount of pressure difference had to be incorporated into the model caused by the way the experimental setup was constructed. Pressures are represented as densities in the LBM, so a slight density difference is accepted to mimic the behavior. Boundaries of the model are adjusted to ensure countercurrent or cocurrent displacement as desired. It was decided to assign the nodes as initial solvent feed or boundary using an image file that was obtained from the corresponding experiment at initial time. The image is modified in order to represent three-node types:—the black pixels would translate as solvent feeding nodes, the gray nodes are the boundaries, and the white nodes are the oil-saturated nodes. For the cocurrent models open-top architecture was simulated as constant pressure (density) on top nodes. The relaxation parameters of the two phases are controlled by the oil viscosity and diffusion coefficient of the solvent, respectively.

B. Diffusion-limited aggregation

The DLA method is a stochastic model which assumes the solvent particles forming the structure wander around randomly before attaching themselves to the structure. One important assumption for this model is that the particles are considered to be in low concentrations, so they do not come in contact with each other and the structure grows one particle at a time rather then by chunks of particles.

The basic DLA algorithm was first described by Witten and Sander [33] and is simple enough to be described informally. Given a discrete 2D grid, a single particle representing the crystal (or aggregate) is placed in the center. This acts as an attraction zone. A particle called the walker is then placed at a random location along the grid perimeter. The particle walks randomly along the adjacent grid cells until it either is adjacent to the chunk or falls of the grid. If it is adjacent to the chunk, it sticks and becomes part of the chunk, thus increasing the size of the attraction zone. A new walker is then inserted at the perimeter and the random walk is repeated.

In order to represent the experimental runs realistically, the attraction zone is assigned to be the lower end of the grid. In real life this would represent the open edge of the model, where solvent is introduced. This is a diversion from the Witten-Sander case, where they modeled diffusion into a particle, and in our case diffusion is through the edge. The rest of the algorithm is loyal to its roots, where the probability may be manipulated using the following modifications.

The first modification applied to this algorithm was to incorporate a sticking probability term to be able to increase or decrease the chance of sticking where particle densities are higher. The method is to introduce probability where the sticking process would normally occur; this increases the chance of sticking for denser zones, where there are more than one adjacent particles, thus more than one chance to stick.

Two other modifications have been applied to take flow and gravity into consideration. The basic principle is to add a velocity vector to the random movement of the walker. In the case of gravity, this is done by adding one unit of velocity that points to Earth. Similarly in the case of flow, the effect can be simulated by adding a velocity vector that is opposite to flow direction.

The time values were obtained from the total number of iterations. The simulations are visually matched with experiments and values yielding the best matches for the kerosene and mineral oil cases are given in Figs. 3(c) and 5(c).

Complexity carried over by probability, diffusion coefficient, and viscosity terms makes it harder to obtain a direct relation for the time value. A curve-fitting approach is applied for the solution. By plotting the number of iterations to achieve an instant of the simulation at matching images with experiments, one can obtain a curve that has the same exponentially increasing behavior as real-time values, to obtain the best match; one only has to multiply with a constant number. In this case, the constant has to be calculated for each experiment done for accurate results. Instead we plotted matching image number versus time values for horizontal and vertical cases. The number of iterations were multiplied by the constant and then plotted. Then, the constant value is changed until a good match is obtained.

Note that the time conversion value based on the number of iterations was obtained using only the horizontal case of the mineral oil for countercurrent transfer. This number was then applied in all the other cases given in Figs. 3–10. Reasonable matches for the times of the experimental results were obtained as shown in those figures, indicating the usability of the conversion factor.

DLA was observed to be a powerful tool for modeling diffusion-dominated phenomena. This was not the case for vertical-oriented samples where the buoyancy (natural convection) caused a dispersive transport dominated by convection.

VII. ANALYSIS OF THE RESULTS AND DISCUSSION

Two different models were utilized to model the transfer of a solvent (that simulates fracture in fractured subsurface reservoirs) into an oil-saturated porous medium (that corresponds to a rock matrix in fractured subsurface reservoirs). Different boundary conditions of the model and orientations and different pairs of fluids were tested. Experimental observations were essential in capturing the physics of the process and critical in developing the algorithms for the above-mentioned numerical models.

It was observed that the DLA model is capable of modeling the horizontal orientations in which only diffusion is the dominating mechanism. The model can accurately reflect the random fingering at early stages [Fig. 4(c)] and the bulk diffusion behavior at later stages for the horizontally oriented samples [Fig. 3(c)]. As this method has no dependence on time and thereby the diffusion coefficient and viscosity, different fluids cannot be modeled by the DLA algorithms. The DLA model in this study was modified to include the boundary effects. This was necessary especially to model the vertically oriented samples, where the process is dominated by buoyant convection [Fig. 5(c)]. The superposition principle was used to introduce sources and sinks to the model. Solvent sources were positioned at the bottom right and left corners of the model, where the sink is positioned in the middle. Locations were chosen to reflect experimental behavior.

The DLA model was partly successful in capturing the physics of the process observed experimentally. It was able to capture the fingering behavior and the front progress in the horizontal cases. As most of the parameters were input by the user, it would not be possible to use this as a reference in the case of a sensitivity analysis. The displacement patterns of the horizontally positioned samples were captured by setting up the initial and boundary conditions observed through the experimental runs. As for the vertical cases, it was difficult to capture the convective behavior and fingering in especially the later stages of the process even though the finger development and front growth at the sides of the model was captured [Fig. 5(c)].

The LBM, on the other hand, was observed as highly applicable and flexible for modeling the miscible interaction between fracture and matrix. The ability to handle complex boundaries was a big advantage of this model. This feature made it possible to simulate cocurrent and countercurrent behavior, as well as the change in transfer mechanism when changing orientation. In the LBM, no user interference to dictate the behavior is present. Instead the user is required to input fluid properties, initial solvent-occupied nodes, and boundary conditions. The model was able to capture the diffusive flow and buoyant convection behavior for vertical [Figs. 5(b), 6(b), 8(b), and 9(b)] and bulk diffusion for horizontally oriented samples [Figs. 3(b) and 4(b)] successfully.

The finger growth after 10 min in case of countercurrent diffusion for kerosene was observed in the LBM simulations (Fig. 5). Two large fingers growing through the sides were prominent and the convective transport was captured in the LBM runs. As for the cocurrent cases, the LBM model for the mineral oil case showed a good match with the experimental observation reflecting the frontal displacement with less fingers (Fig. 9). The finger growths and the buoyant convective transport were captured successfully. In the kerosene case, however, thin fingers were not observed in the LBM simulations [between 11 and 32 min in Fig. 8(a)], but

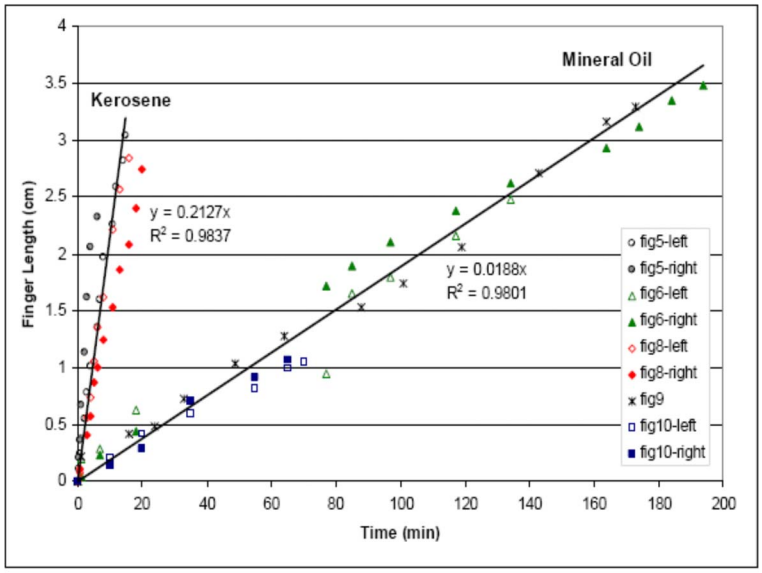

FIG. 13. (Color online) Displacement versus time plot of observed fingers for five vertical experiments.

the convective transport was reflected well and the time matches were successful (Fig. 8).

Square-shaped models were used in all experiments. In order to minimize the boundary effects that caused a faster movement of the front through the less resistant portion (the two sides of the models) on the process, a different model dimension was applied. An extreme case with 2:1 aspect ratio was also included [Fig. 10(a)] in an effort to see the adaptability of the LBM proposed in this study [Fig. 10(b)]. No input parameters were changed except the dimensions of the model. This turned out to be a test of the algorithm and time conversion factor presented in this paper on a different shape and dimension model. In this case the effect of boundaries was suppressed because of the width of the model. Initial fingering caused by initial random walk of diffusion was obvious before the gravity effect starts to become dominant. The process was observed to be similar to double-diffusive fingering. At the later stages, the buoyant convection for the unswept parts was also visible. Despite the high aspect ratio (or shorter size) of the sample, the accumulation of the lighter phase on top of the model causing buoyant convection was observed after 76 min (Fig. 10). The LBM model proposed was able to simulate the process successfully as can be seen through the comparison of the simulation and experimental runs.

Note that the porous medium characteristics of the model have not been taken into account in this study. The relatively simple design of the model (homogeneous and unconsolidated design of the same size of standard glass beads) made this assumption valid. Inclusion of the characteristics of natural porous medium is still a challenge for the LBM modeling. There are studies to include the effect of pore media, in a manner that low-resolution, low-grid-size simulations can be run [34,35]. Although these studies are useful at the macroscale, it would not be possible to model fingering behavior observed in the experimental part of this study using grain size grids. It is possible to run the LBM model through real pore structure; however, vast computing power and real digitized rock structure is required.

The LBM is well suited to model dispersion, particularly in the intermediate Peclet (defined as WU/D_m where W is the width, U is the velocity, and D_m is the diffusion coefficient) number range. This corresponds to the region where neither diffusion nor fluid flow dominates the spreading of solute. It is time dependent, and viscosity and diffusion coefficient changes can be accurately reflected in this model. Since the LBM is required to be scaled accordingly for the constraints of the algorithm, time has to be scaled back to real-time simulation values. This is done using Eq. (21).

Experiments in the horizontal orientation and the initial stage for vertical-oriented samples were purely diffusion dominated. The random behavior observed in these processes was captured to some extent as can be seen through the comparison of the experimental and stochastic images. This was achieved by capturing the random walk stage at the early times of the process visually, and the LBM was applied just at the end of this step. This typically corresponds to the first few minutes of each experiment. Solvent was fed through these nodes initially to create the disturbance, which is believed to be affecting the overall behavior. As diffusion loses its dominant power, the nodes previously invaded by random walk became the paths for solvent feed.

VIII. QUANTITATIVE ANALYSIS OF EXPERIMENTAL OBSERVATIONS

Finally, in an effort to provide a more quantitative analysis, a finger displacement versus time plot obtained from experimental runs is given in Fig. 13. The slope of this plot would give the speed of the fingers. Since most of the figures consisted of two major fingers growing through each side of the model, both fingers (named "left" and "right" fingers) were considered in this plot. Two groupings were observed based on the viscosity of the fluids: namely, kerosene or mineral oil. The constant speed for fingers in kerosene was measured to be 0.127 m/sec whereas the fingering speed drops to 0.011 m/sec for the higher-viscosity mineral oil

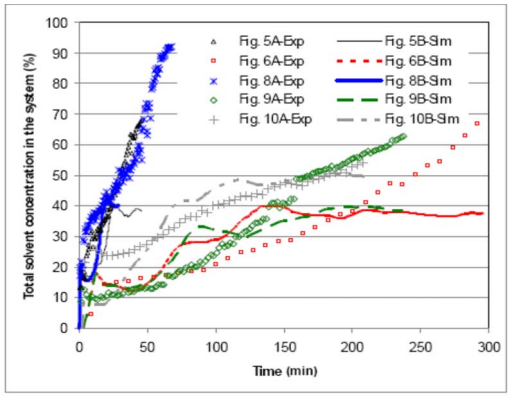

FIG. 14. (Color online) Comparison of the total areas covered by the solvent (or total solvent concentration in the system) for five vertical cases. Symbols and lines represent the experimental and LBM model results, respectively.

sample. Interestingly, the boundary conditions are not observed to affect the finger speed.

In addition to the speed of the fingers, we analyzed the area invaded by the solvent quantitatively and compared the experimental and the LBM model results (Fig. 14). In this exercise, the concentration of the solvent in each grid (pixel) was calculated based on the "gray level" which is obtainable from the LBM model. A fully solvent filled grid will have a value of 255 (pure red color). Zero corresponds to the "no solvent in the grid" case. This was a relatively easier exercise for the LBM simulations as a color code indicating the amount of solvent in the grid could be obtained at any time. For the experimental cases, however, a threshold color level was set and anything above the threshold corresponds to the solvent-filled case.

The results are highly consistent except the very-late-time data. The late-time inconsistency is due to using a threshold value for the experimental case rather than a color code between 0 and 255 as in the LBM case. The late-time consistency is more conspicuous in the two kerosene cases (Figs. 5 and 8). For example, the snapshot at 43 min for the kerosene diffusion case given in Fig. 5(a) or the snapshot at 68 min for the kerosene diffusion case given in Fig. 8(a) shows a totally solvent-swept model (almost 100%-solvent-filled case). But as can be distinguished by the color contrast visually, it is not purely solvent color (dark red), but it has some "pinkish gray tones," especially at the center of the two models. Those regions indicate not-totally solvent-filled portions, but depending on the selection of the threshold value, some portions in that region could have been assumed to be 100% solvent. The comparison for the models in general showed that the experimental and LBM results are consistent especially at early and middle times at which the major finger development and sweep take place.

IX. CONCLUSIONS AND REMARKS

Bulk diffusion was observed in the horizontal experiments where there was no gravity effect. The frontal progress of the diffusion front was prominent and the fronts, regardless of the boundaries, proceeded as a bullet-shaped profile. Diffusion was the dominating mechanism during this process. Two different viscosity fluids did not exhibit much difference in terms of fingering and front movement since the diffusion coefficients were close to each other. The DLA and LBM models were both successful in capturing the physics of the process for the horizontal cases.

Vertically positioned models showed a "convective" displacement characteristics caused by the gravity effect. This effect is more prominent in case of kerosene (especially for the cocurrent interaction) as the gravity- (buoyancy-) driven dispersion and finger development was more severe and the progress of the front was much faster compared to the mineral oil case. Depending on the fluid properties, the displacement process might diverge from convective to frontal displacement. The cocurrent mineral oil-pentane (frontal progress of the front) and kerosene (severe fingering and the process strongly controlled by convective displacement) cases were the typical example for this situation.

Viscosity, orientation, and density were observed to be critical to the fingering. The most significant fingering was obtained in the case of kerosene-pentane displacement in the vertical direction, especially for the cocurrent models. For all different boundary conditions, the kerosene cases yielded a much faster process than the mineral oil, indicating the effect of viscosity on the displacement process.

The DLA-type modeling was chosen as a starting point. It was quite suitable for the horizontal (bulk) diffusion process since this is a diffusion-dominated process. The controlling parameter for this process is observed to be the diffusion coefficient. Once the iteration-time relationship was established, it was applied successfully for the horizontally oriented samples.

For the vertically oriented samples, however, a more powerful tool is required. The LBM was chosen due to its capability in handling complex boundaries and accuracy for the processes near the intermediate Peclet number region. Although the model was not as accurate in terms of randomness and small fingers on horizontal orientation, it showed a reasonable match for the later stages of the process [Figs. 3(b) and 4(b)]. The LBM was also successful in capturing the convective-type process and the immediate change from diffusion to dispersion (natural convection and diffusion) was achieved just with the introduction of gravity term [Figs. 5(b), 6(b), 8(b), and 9(b)].

Since it was apparent that the gravity term was the most important parameter for the vertically oriented samples, it had to be fine-tuned for different fluids and boundary conditions. For the kerosene cases, the less-gravity effect was applied compared to mineral oil due to a lower density difference. The less-gravity effect and less-viscous oil phase translate into more fingering and faster transfer by convection for both cocurrent and countercurrent cases [Figs. 5(b) and 8(b)]. The difference between the mineral oil and kerosene cases can be successfully reflected by changing the viscosity and gravity terms.

The cocurrent cases were simulated by assigning constant pressure at the top of the model and this was achieved by assigning the top nodes to constant density. The low-pressure zone at the top of the models magnified the effect of gravity

especially for mineral oil. The mechanism was not convection for the whole life of the process. It starts as diffusion initially for a short time, then converts into dispersive flow (natural convection due to gravity and diffusion) [Figs. 8(b) and 9(b)].

Finally, the major assumptions, limitations, and strengths of the modeling study presented in this paper are listed below.

(i) No characteristics of porous medium were included in the modeling study. The process time and type are dependent on the pore structure and heterogeneity and this constitutes the next phase of the study,

(ii) The transfer process starts as a random—diffusion—process. The LBM is not so strong to model this process. To preserve accuracy at later stages, solvent is fed into model through the randomly invaded nodes. After filling a few layers of pores through this process with a random displacement process, the LBM algorithm is started.

(iii) The finger development at early stages and the dispersive flow (natural convection due to gravity and diffusion) process were captured in all cocurrent and countercurrent interaction cases regardless the orientation and fluid viscosity.

(iv) The DLA modeling was limited to horizontal case and the model was not capable of reflecting the gravity and viscosity effects. It however successfully captured the random fingering process and later diffusion for the horizontal cases.

(v) The time conversion value was observed quite universal.

(vi) Using microscale phenomena the macroscale behavior was captured by the LBM modeling. Note that the LBM approach presented a modeling technique that does not require any further input based on experimental observations and/or semiempirical correlations. In the modeling study, only the viscosity term and the boundary conditions were input and the gravity term was added if it is vertical displacement. The only assumption was the one given in item (ii).

ACKNOWLEDGMENTS

This study was partly funded by two NSERC Grants (No. G121210595 and Strategic Grant No. G121990070). The funds for the equipment used in the experiments were obtained from the Canadian Foundation for Innovation (CFI) (Project No. 7566) and the University of Alberta. We gratefully acknowledge these supports. The first author (C.U.H.) also thanks Harlan W. Stockman for valuable discussions.

[1] R. Lenormand, J. Phys.: Condens. Matter **2**, 79 (1990).
[2] D. Wilkinson, Phys. Rev. A **30**, 520 (1984).
[3] G. Wagner, P. Meakin, J. Feder, and T. Jossang, Physica A **264**, 321 (1999).
[4] R. Lenormand, Proc. R. Soc. London, Ser. A **423**, 159 (1989).
[5] L. Kadanoff, Phys. Today **39**(9), 7 (1986).
[6] R. Benzi, S. Succi, and M. Vergassola, Phys. Rep. **222**, 145 (1992).
[7] D. H. Rothman and S. Zaleski, Rev. Mod. Phys. **66**, 1417 (1994).
[8] S. Chen, S. P. Dawson, G. D. Doolen, D. R. Janecky, and A. Lawniczak, Comput. Chem. Eng. **19**, 617 (1996).
[9] G. D. Doolen and S. Chen, Annu. Rev. Fluid Mech. **30**, 329 (2001).
[10] A. Birovljev, L. Furuberg, J. Feder, T. Jossang, K. J. Maloy, and A. Aharony, Phys. Rev. Lett. **67**, 584 (1991).
[11] M. Ferer, G. S. Bromhal, and D. H. Smith, Phys. Rev. E **67**, 051601 (2003).
[12] J. F. Fernandez, R. Rangel, and J. Rivero, Phys. Rev. Lett. **67**, 2958 (1991).
[13] M. Bouzidi, M. Firdaouss, and P. Lallemand, Phys. Fluids **13**, 3452 (2001).
[14] E. G. Flekkoy, Phys. Rev. E **47**, 4247 (1993).
[15] H. W. Stockman, R. J. Glass, C. A. Cooper, and H. Rajaram, Int. J. Mod. Phys. C **9**, 1 (1998).
[16] N. Takada, M. Misawa, A. Tomiyama, and S. Hosokawa, J. Nucl. Sci. Technol. **38**, 330 (2001).
[17] C. U. Hatiboglu and T. Babadagli, *CIM 56th Annual Technical Meeting, Canadian International Petroleum Conference* (Calgary, Canada, 2005).
[18] C. U. Hatiboglu and T. Babadagli (unpublished).
[19] C. U. Hatiboglu and T. Babadagli, *2005 SPE Annual Technical Conference and Exh.* (Dallas, TX, 2005).
[20] S. E. Pringle, R. J. Glass, and C. A. Cooper, Transp. Porous Media **47**, 195 (2002).
[21] R. A. Wooding, J. Fluid Mech. **7**, 501 (1960).
[22] A. K. Gunstensen, D. H. Rothman, S. Zaleski, and G. Zanetti, Phys. Rev. A **43**, 4320 (1991).
[23] D. H. Rothman and J. M. Keller, J. Stat. Phys. **52**, 1119 (1988).
[24] A. Cali, S. Succi, A. Cancelliere, R. Benzi, and M. GramignaniPhys. Rev. A **45**, 5771 (1992).
[25] N. S. Martys and H. Chen, Phys. Rev. E **53**, 743 (1996).
[26] I. W. Yeo and S. Ge, Geophys. Res. Lett. **28**, 3983 (2001).
[27] E. G. Flekkoy, U. Oxaal, J. Feder, and T. Jossang, Phys. Rev. E **52**, 4952 (1995).
[28] X. Shan and G. Doolen, J. Stat. Phys. **81**, 379 (1995).
[29] I. Ginzbourg and P. M. Alder, J. Phys. II **4**, 191 (1994).
[30] X. He, Q. Zou, L. S. Luo, and M. Dembo, J. Stat. Phys. **87**, 115 (1997).
[31] J. M. Buick and C. A. Greated, Phys. Rev. E **61**, 5307 (2000).
[32] R. G. M. Van Der Sman, Phys. Rev. E **74**, 026705 (2006).
[33] T. A. Witten and L. M. Sander, Phys. Rev. Lett. **47**, 1400 (1981).
[34] M. Yoshino and T. Inamuro, Int. J. Numer. Methods Fluids **43**, 183 (2003).
[35] O. Dardis and J. McCloskey, Phys. Rev. E **57**, 4834 (1998).